Report for SC-2208 experiment

Uri Raviv

To polymerize microtubule (MT) at the beamline, tubulin concentrated to 45±5 μM in PEM buffer (50 mM 1,4- piperazinediethanesulfonic acid, 1 mM $MgCl_2$, 1mM EGTA, 0.02 % (w/v) NaN_3, adjusted to pH = 6.8 with ca. 70 mM NaOH), 1 mM GTP and 5 % glycerol was incubated at 36±1 ^oC for 20min. MT depolymerization was suppressed by adding the chemotherapy drug Taxol at 1:1 tubulin to Taxol mole ratio. We also checked that 0.1 wt% of Glutaraldehyde of preassembled MT (at home) did not have a detectable effect on the MT scattering data. Other drugs were examined as well and the results are still being analyzed. We have also examined the sample damage in the various modes of measurements and concluded that working with capillaries in this beamline gives very good data if scanned for 5 min. We also tried various ways to hold the sample in the beam and improved the design of our capillary sample holder based on the experience from our July 2007 run.

The SAXS profile of MTs is consistent with the form factor of an isotropic hollow cylinder (Fig. 1). Based on MT structural data (1, 2), we modeled the MT as three concentric cylindrical shells, of a high electron density region surrounded by two low ones, as shown in the inset to Fig. 1, keeping the total wall thickness, $a_1 = 4.9$ nm, and mean electron density as those of MTs. The thickness and location of the high electron density region, within the MT wall, and the inner MT radius, R_{in}, are fitting parameters in this model (see details below).

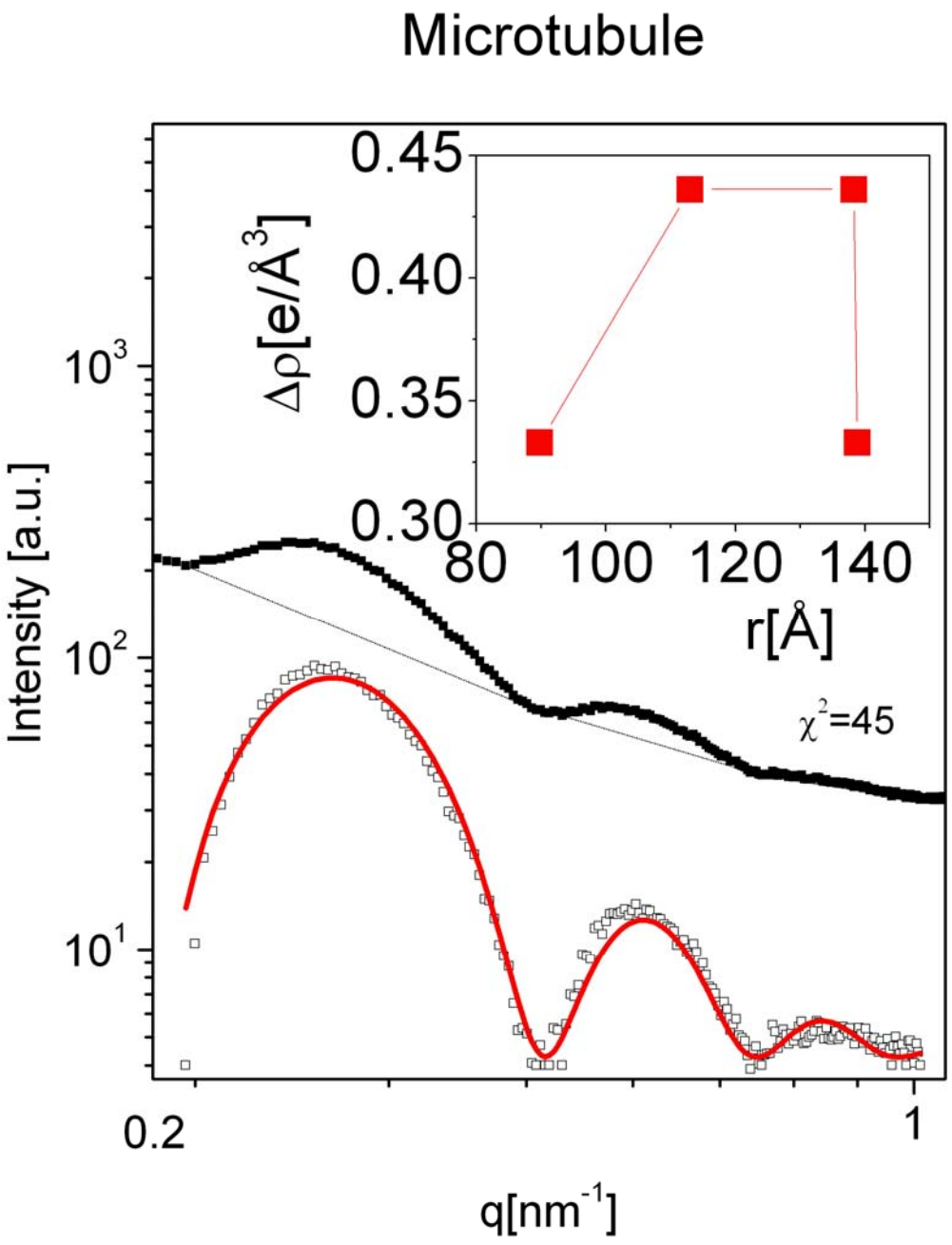

Figure 1.

Pure MT data and analysis. The solid symbols show the azimuthally averaged raw MT SAXS data. The thin broken black line is a series of power laws that pass through the minima of the scattering intensities. As in other MT-related scattering studies(3-6), this is the assumed background scattering. Open symbols show the MT SAXS data, following background subtraction. The red solid curve is the fitted scattering model. The inset shows the variation of the radial electron density, $\Delta\rho(r)$, relative of the MT wall, as obtained from fitting the data to the model of isotropic infinitely long hollow cylinders with non-uniform electron density profile. *r* is the distance from the center of the cylinders

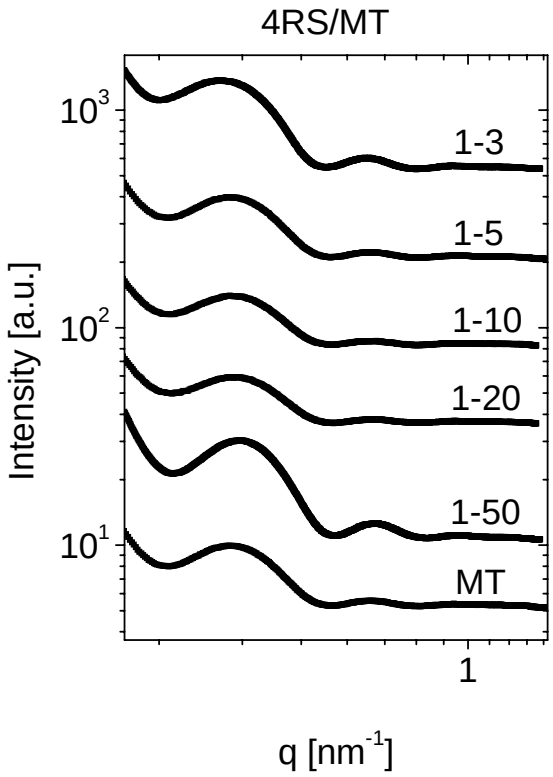

Figure 2. Azimuthally averaged raw MT – tau (4RS isoform) complexes data, at tau-tubulin molar ratio as indicated in the figure.

We then looked at MT- tau (isoform 4RS) complexes (Figure 2) we found that the solution x-ray scattering is extremely sensitive to very small changes in the tau/tubulin stoichiometry. We then looked at other MT-tau complexe (other tau isoforms) and found detectable differences between MT-tau complexes formed with different tau isoforms. Based on analysis similar to that shown in Figure 1 we plot in Figure 3 the variation of the inner tau radius as a function of the tau/tubulin molar ration for 4 tau isoforms. The data show that even small amounts of tau can influence the size of MTs. Different tau isoforms change the MT size to a different extent. The isoforms with 4 binding domain (4RS and 4RL isoforms) have a greater effect on the MT size than the isoforms with 3 binding domains (3R isoforms). Unexpectedly the short projection domains (3RS and 4RS) induce smaller MT size changes than their corresponding long projection domain analogue (3RL and 4RL).

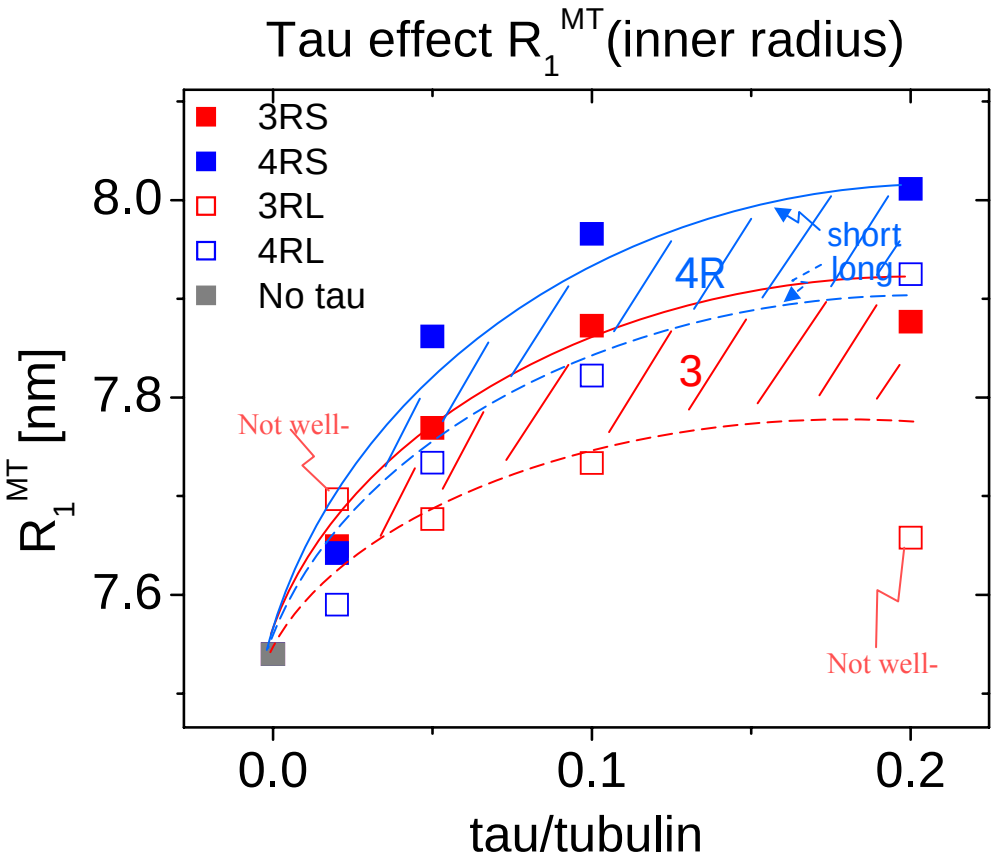

Figure 3. Inner MT radius (R_1^{MT}) as a function of the tau/tubulin molar ratio (in moles) of different tau isoforms (as indicated in the figure).

Details about MT data analysis

To analyse the data, we start by considering the form factor of a single hollow cylinder of core radius R_c and a shell radius R_s and a total height of $2H$. We assume that the inside and outside of the tube have the same electron density and the inside of the tube has a uniform electron density that differ by $\Delta\rho_0$ from the outside of the tube. The scattering amplitude F is proportional to the Fourier transform of the electron density of the hollow cylinder:

$F(q_\perp,q_z) \propto \int_V \Delta\rho_0(r)\exp(-iq\cdot r)dr$, where the integration is over the volume V of the hollow cylinder.

In cylindrical coordinates we obtain:

$$F(q_\perp,q_z) \propto \Delta\rho_0 \int_{-H}^{H} dz \exp(-iq_z z)\int_{R_x}^{R_s} \rho d\rho \int_0^{2\pi} \exp(-iq_\perp \rho\cos(\phi)d\phi$$

$$= 4\pi\Delta\rho_0 \sin(Hq_z/q_z)\int_{R_c}^{R_s} \rho d\rho J_0(q_\perp\rho) = \ 4\pi\Delta\rho_0 \sin(Hq_z/q_z)\{R_s J_1(q_\perp R_s) - R_c J_1(q_\perp R_c)\},$$

where J_0 and J_1 are the zero and first Bessel functions of the first kind.

The intensity I is given by $|F|^2$, but since our solutions are isotropic we need to perform a powder average in the reciprocal q space:

$$I(q) \propto \int |F|^2 d\Omega_q = \int_0^{2\pi} d\psi_q \int_0^{\pi} |F|^2 \sin\theta_q d\theta_q = 2\pi \int_0^{\pi} |F|^2 \sin\theta_q d\theta_q$$

By setting $x = \cos\theta_q$ we get: $q_\perp = q\sin\theta_q = q(1-x^2)^{1/2}$ and $q_z = q\cos\theta_q = qx$ so finally the intensity is given by:

$$I(q) = A(\Delta\rho_0)^2 \int_0^1 \frac{\sin^2(Hqx)}{q^4x^2(1-x^2)}\{R_s J_1(qR_s(1-x^2)^{1/2}) - R_c J_1(qR_c(1-x^2)^{1/2})\}^2 dx + B$$

where A and B are constants.

In the more general case we have a series of n concentric homogenous hollow cylinders with an overall radial electron density profile given by the set of parameters (R_k , ρ_k, H_k). $(\rho_{k+1} + \rho_k)/2 = \Delta\rho_k$ is the difference between the electron density of the surrounding (the solvent in our case) and the k-th homogenous hollow cylinder with a core radius R_k and a shell radius R_{k+1}. $2H_k$ is the height of the k-th hollow cylinder (H_{n+1}=0) and $k=1,2,\ldots,n+1$. The scattering intensity of such randomly oriented n concentric cylinders is:

$$I(q) = A\int_0^1 \frac{1}{q^4x^2(1-x^2)}\left(\sum_{k=1}^{n} \sin(H_k qx)\cdot\Delta\rho_k \cdot \left\{R_{k+1}J_1\left(qR_{k+1}(1-x^2)^{1/2}\right) - R_k J_1\left(qR_k(1-x^2)^{1/2}\right)\right\}\right)^2 dx + B$$

For n infinitely long concentric hollow cylinders we get:

$$I(q) = A\int_0^1 \frac{1}{q^4x^2(1-x^2)}\left(\sum_{k=1}^{n} \Delta\rho_k \cdot \left\{R_{k+1}J_1\left(qR_{k+1}(1-x^2)^{1/2}\right) - R_k J_1\left(qR_k(1-x^2)^{1/2}\right)\right\}\right)^2 dx + B$$

In our case we reduced the number of parameters by having R_k , ρ_k be a function of a subset of parameters a_i out of which a much smaller subset of parameters was free to float.

For the case of pure microtubule solutions we have the set of parameters shown in the Table 1. The values of R_k and ρ_k are calculated (based on the parameters of Tables I) as described in Table II.

Table I. The values of a_i in the case of pure MT.

Parameter value	Description	Source
a_1 = 8.97 nm	R_1 - the internal microtubule radius	Tubulin structural data(1) but allowed to fluctuate within reasonable physical limits
a_2 = 2.31 nm	$R_2 - R_1$ - width of the internal low electron density region	Free
a_3 = 2.52 nm	$R_3 - R_2$ - width of the high electron density region	Free
a_4 = 4.9 nm	$R_4 - R_1$ - total microtubule wall width	Tubulin structural data(1)
a_5 = 411 e/nm^3	Mean electron density of microtubule wall	Microtubule(1) and tubulin(7) structural data, tubuline M_w and partial specific volume(2, 8)

Table II. Calculation of R_k and ρ_k

R_k	ρ_k
$R_1 = a_1$	$\rho_1 = 0$
$R_2 = a_1 + a_2$	$\rho_2 = 2(a_6 - a_{10})a_4/(a_3 + a_4)$
$R_3 = a_1 + a_2 + a_3$	$\rho_3 = \rho_2$
$R_4 = a_1 + a_4$	$\rho_4 = \rho_1$

References

1. Li, H., D. J. DeRosier, W. V. Nickolson, E. Nogales, and K. H. Downing. 2002. Microtubule Structure at 8 Å Resolution. Structure 10:1317-1328.
2. Lee, J. C., R. P. Frigon, and S. N. Timasheff. 1973. The Chemical Characterization of Calf Brain Microtubule Protein Subunits. J. Biol. Chem. 248:7253-7262.
3. Needleman, D. J., M. A. Ojeda-Lopez, U. Raviv, H. P. Miller, L. Wilson, and C. R. Safinya. 2004. Higher-order Assembly of Microtubules by Counterions: From Hexagonal Bundles to Living Necklaces. Proc. Natl. Acad. Sci. USA 101:16099-16103.
4. Fernando-Diaz, J., J. M. Andreu, G. Diakun, E. Towns-Andrews, and J. Bordas. 1996. Structural Intermediates in the Assembly of Taxoid-Induced Microtubules and GDP-Tubulin Double Rings: Time-Resolved X-ray Scattering. Biophys. J. 70:2408-2420.
5. Andreu, J. M., J. Bordas, J. F. Diaz, J. Garcia de Ancos, R. Gil, F. J. Medrano, E. Nogales, E. Pantos, and E. Towns-Andrews. 1992. Low Resolution Structure of Microtubules in Solution:

Synchrotron X-ray Scattering and Electron Microscopy of Taxol-induced Microtubule Assembled from Purified Tubulin in Comparison with Glycerol and MAP-induced Microtubules. J. Mol. Biol. 226:169-184.

6. Raviv, U., D. J. Needleman, Y. Li, H. P. Miller, L. Wilson, and C. R. Safinya. 2005. Cationic Liposome - Microtubule Complexes: Pathways to the Formation of Two State Lipid-Protein Nanotubes with Open or Closed Ends. Proc. Natl. Acad. Sci. USA 102:11167-11172.
7. Nogales, E., S. G. Wolf, and K. H. Downing. 1998. Structure of αβ tubulin dimer by electron crystallography. Nature 393:199-203.
8. Frigon, R. P., and S. N. Timasheff. 1975. Magnesium-induced self-association of calf brain tubulin. I. Stoichiometry. Biochemistry 14:4559-4566.